A Process-based Model for Quantifying the Impact of Climate Change on Permafrost Thermal Regimes

Yu Zhang, Wenjun Chen, and Josef Cihlar

Canada Centre for Remote Sensing,
Natural Resources Canada,
588 Booth Street,
Ottawa, ON, Canada, K1A 0Y7

Submitted to: ***Journal of Geophysical Research***

Corresponding author:

Yu Zhang
Environmental Monitoring Section
Canada Centre for Remote Sensing
Natural Resources Canada
588 Booth Street, 4th floor
Ottawa, Ontario
Canada, K1A 0Y7
Tel: 1-(613) 947-1367
Fax: 1-(613) 947 1383
E-mail: yu.zhang@ccrs.nrcan.gc.ca

Abstract. Air temperature at northern high latitudes has increased at a higher rate than the global mean in the last century and most GCMs projected that this pattern will continue. Climate warming can increase summer thaw depth and induce permafrost degradation, which may alter the dynamics and functions of northern ecosystems and the lifestyles of northern residents. To address these issues, we developed a process-based model to simulate permafrost thermal regimes by combining the strength of existing permafrost models and land surface process models. Soil temperature and active-layer thickness were simulated by solving the heat conduction equation, with the upper boundary conditions being determined using the surface energy balance, and the lower boundary conditions being defined as the geothermal heat flux. The model integrated the effects of climate, vegetation, ground features and hydrological conditions based on energy and water transfer in the soil-vegetation-atmosphere system. The model was validated against the measurements at four sites in Canada. The simulation results agreed with the measurements of energy fluxes, snow depth, soil temperature and thaw depth. These results indicate that this physically based model captured the effects of climate, vegetation and ground conditions on soil temperature and freezing/thawing dynamics, and the model is suitable to investigate the impacts of transient climate change on soil thermal regimes and permafrost degradation, and their consequent effects on ecosystem dynamics.

Keywords: Model; Soil temperature; Active-layer thickness; Permafrost; Climate change.

1. Introduction

Air temperature at northern high latitudes, over the period of instrumental records, has increased at a higher rate than the global mean, and most GCMs projected that this pattern will continue [*Houghton et al., 1996; Zhang et al., 2000; Anisimov, 2001*]. As air temperature increases, permafrost may warm and thaw, and summer thaw depth may increase [*Nelson, 2003*]. This may change the dynamics and functions of northern ecosystems, and release to the atmosphere of a fraction of the large amount of carbon stored in the frozen soils, which can further enhance climate warming [*Oechel et al., 1993; Trumbore et al., 1996; Goulden et al., 1998; Serreze et al., 2000; Anisimov et al., 2001*]. Increases in active-layer thickness (ALT) and permafrost degradation may also bring about land surface subsidence, which can damage building foundations, roads, and pipelines, and impact on the lifestyles of northern residents, who have adapted to the permafrost environment over centuries [*Anisimov et al., 2001; Nelson et al., 2001; 2002*]. To address this issue, the Global Terrestrial Network for Permafrost (GTN-P) [*Burgess et al., 2000*] has been established to monitor the responses of permafrost thermal regimes to climate change, including changes in active layer thickness and ground temperature [*Brown et al., 2000*]. It is essential, however, to develop dynamic models based on these measurements so that we can assess the transient responses of permafrost conditions to climate change, including the interactions among soil, vegetation and climate.

A wide spectrum of models has been developed and applied to quantify the effects of climate and its impact on permafrost conditions [*Goodrich, 1982; Nelson, 1986; Bonan, 1989; Smith and Riseborough, 1996; Anisimov and Nelson, 1996; Anisimov et al., 1997; Nelson et al., 1997; Romanovsky and Osterkamp, 1997; Smith and Burgess, 1998; Malevsky-Malevich, et al., 2001*]. One type of models relies on empirical or simplified analytical relationships between soil temperature (or thaw depth) and air temperature and other variables that are more widely available. For example, *Brown* [*1970*] estimated mean annual soil temperature from mean annual air temperature in delineating permafrost distributions. *Romanovsky and Osterkamp* [*1997*] and many others [*e.g., Nelson, 1986; Bonan, 1989; Nelson et al., 1997*] estimated ALT based on accumulated air temperature or the degree-day approach. This type of models generally needs less input data and is

efficient in calculation, but it cannot be applied to time-dependant analyses (e.g., the impacts of transient climate change) because it uses an assumption of stationarity or equilibrium without explicitly considering the heat exchange processes [*Burn and Smith, 1993*]. Another type of models simulates soil temperature and ALT by solving the heat conduction equation, and thus has the potential for transient analyses [*e.g., Goodrich, 1982; Kane et al., 1991; Malevsky-Malevich, et al., 2001*]. However, most models of this type use air temperature to estimate surface temperature for the upper boundary conditions without explicitly considering energy exchange processes, and treat snow depth and snow density as inputs. Because the relationship between air temperature and soil surface temperature can differ significantly under different soil, vegetation and moisture conditions [*Chen et al., 1997a; 1997b; Blanken et al., 1998*], soil thermal regimes can be very different under the same macroclimate conditions [*Smith, 1975*]. For this reason, *Anisimov* [*1989*] and *Waelbroeck* [*1993*] used simplified approaches of the surface energy balance to simulate soil thermal dynamics of permafrost, and consider the effects of snowpack and soil moisture. In recent decade, the interactions among soil, vegetation and hydrology has been studied intensively and modeled successfully based on water and energy transfer in soil-vegetation-atmosphere systems (SVATS) [*e.g., Sellers et al., 1997; 1986; Verseghy, 1991*]. These models were developed mainly to provide surface boundaries for GCMs, and generally consider a shallow soil profile. They are not suitable for direct applications in simulating permafrost related processes (e.g., thawing and freezing, ALT, excess ice and ground subsidence), because these processes and their change with time are involved in a much deeper soil profile.

In this study, we combined the strength of existing permafrost models and SVATS models to develop a physically based model of Northern Ecosystem Soil Temperature (NEST). We used a process-based approach so that the effects of climate, vegetation, ground features and hydrological dynamics can be quantified and integrated based on energy and water transfer in the soil-vegetation-atmosphere systems. Details of the model are described in Section 2, followed by validation and sensitivity analysis in Section 3. Results of applying NEST to a region in western Canada are reported in a companion paper [*Chen et al., this issue*].

2. Model Description

2.1. General structure

Permafrost, as a special thermal condition of ground, changes spatially and temporally with climate and local conditions. Several important features of northern ecosystems are closely related with the soil thermal dynamics, and need to be addressed explicitly in the model. These features include: thawing and freezing cycles in the top layers underlain by frozen layers, unfrozen layers, or a combination of frozen and unfrozen layers, snowpack dynamics, organic materials on top of the mineral soils, excess ice in permafrost layers and ground subsidence when excess ice melts. Vegetation influences soil thermal dynamics by its effects on surface energy and water fluxes and on soil moisture conditions. Therefore, we consider soil, vegetation and the atmosphere as an integrated system. The vertical profile of heat conduction includes snowpack, forest floor, peat layers, mineral soils and bedrock (Figure 1A). We assume these components are horizontally uniform within a simulation unit, so that soil thermal dynamics can be determined by vertical energy and water fluxes. The top organic layers are considered as forest floor. When organic layers are deep (e.g., deeper than 20 cm), organic layers under the forest floor are considered as peat layers. Beneath the mineral soils is bedrock, in which we assume there is no water flux.

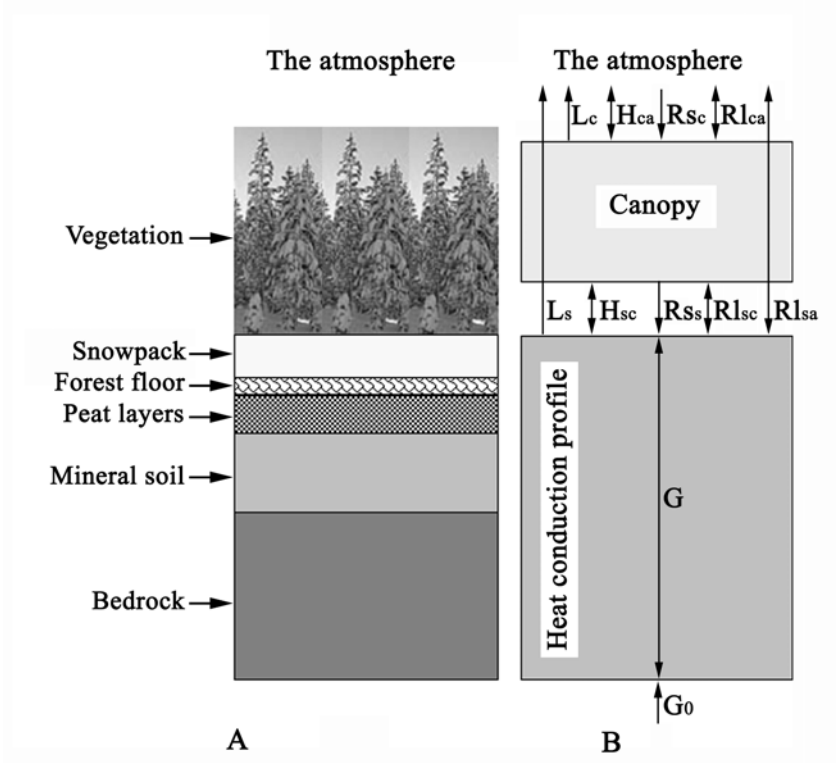

Figure 1. A) The components of the system considered in the NEST model, and B) energy fluxes between soil, vegetation and the atmosphere. L, H, Rs, Rl and G are the latent heat flux, sensible heat flux, solar radiation, long-wave radiation, and conductive heat flux, respectively. The subscripts are to identify these fluxes between different components (s, c and a for ground surface, canopy and the atmosphere, respectively). G_0 is the geothermal flux.

Figure 1B shows the energy fluxes between soil, vegetation, and the atmosphere. The thermal dynamics of the ground and snow layers are determined by numerically solving the one-dimensional (vertical direction) heat conduction equation (Eq. 1. The equations are listed in table 1, and the definitions of the variables are listed in the notation), including an internal heat source or sink term [*Patankar, 1980*]. Convective heat transfer with water flux is not considered in the model. The heat conduction equation is solved numerically by converting it to an explicit form (Eq. 2-4), which is more efficient for calculation and for directly considering the effects of thawing/freezing processes. The ground profile (including forest floor, peat layers, mineral soil layers, and bedrock layers) is divided into 40 layers and the thickness of the layers gradually increases from 0.1 m for top layers to 2 m close to the lower boundary at 35 m depth. The snowpack is also divided into about 0.1 cm layers, and the number of snow layers and the thickness the snowpack are updated based on snow dynamics. We use time steps of 30 minutes or less so that the calculation is stable. Heat capacities of ground and snow layers are calculated from the specific heat capacity of liquid water, ice, organic materials, minerals and air, weighted according to their respective volumetric fractions (Eq. 5). The thermal conductivity of each ground layer is calculated as the geometric mean of the thermal conductivities of the constituents (Eq. 6) [*Johansen, 1975*]. The thermal conductivity of each snow layer is estimated based on its density (Eq. 7)[*Mellor, 1977*].

To solve the heat conduction equation (Eq. 1), we need to define the upper and lower boundary conditions, to consider snow dynamics (changes in thickness and density), to track the changes in soil thermal properties, and to include the effects of freezing and thawing. The lower boundary is defined as the geothermal flux. Currently the lower boundary is set at 35 m below the ground surface, but a deeper boundary can be selected in the model if needed. The upper boundary surface for heat conduction (below referred as the HC upper surface) is the ground surface or the surface of the snowpack if snowpack is present. Section 2.2 describes the upper boundary conditions determined based on energy balance; Section 2.3 considers the effects of plant canopy on soil moisture and the energy exchange between the HC upper surface and the atmosphere, followed by discussions of hydrology related processes, including water input, output, and distribution in soil profile (Section 2.4), snow dynamics (Section 2.5), thawing and

freezing (Section 2.6), and ground subsidence if excess ice in permafrost melts (Section 2.7). All these processes are integrated in terms of energy and water transfer in the soil-vegetation-atmosphere system.

2.2. The upper boundary conditions

The upper boundary conditions are determined based on the energy balance on the HC upper surface (Eq. 8). The vegetation area index (*VAI*) influences both solar radiation and long-wave radiation on the surface (Eq. 9 and 10). *VAI* includes the effects of foliage, branches and boles. We estimate the contribution of branches and boles to *VAI* as 10% of the summertime leaf area index [*Gower et al., 1997*]. The emissivity of air depends on air temperature and cloudiness (Eq. 11 and 12) [*Unsworth and Monteith, 1975; Campbell, 1977*].

We use air temperature above the canopy to estimate sensible heat flux above the HC upper surface (Eq. 14), because measurements show that sensible heat exchange within canopy is often counter-gradient [*Blanken et al., 2001; Chen et al., 1997a*], mainly associated with large-scale coherent eddies, which regularly replace the canopy air with the "fresh" air above the canopy [*Chen et al., 1997a; 1997b*].

The aerodynamic resistance between the canopy and the air above the canopy (r_{aa}) is estimated based on *Choudhury and Monteith* [*1988*] (Eq. 15-17). The zero plane displacement and the roughness height are estimated based on the canopy height [*Campbell, 1977*]. The aerodynamic resistance between the canopy and the HC upper surface is estimated by the same method as for r_{aa}, but using the temperatures of the canopy and the HC upper surface, and wind speed in the canopy.

The heat flux from the HC upper surface to the underlying layer is estimated based on the temperature gradient between the surface and the upper soil or snow layer (at mid point of the layer) (Eq. 18). The latent heat flux is estimated based on Penman-Monteith equation [*Monteith, 1965*] (Eq. 19). The surface resistance (r_s) is estimated based on soil moisture [*Sun, 1982*]. r_s is set as 0 $s \cdot m^{-1}$ if the surface is covered by snow.

The HC upper surface temperature is determined by iterative calculation of the surface energy balance, and then the surface heat flux to soil or snow profile can be determined. If snow is present and the calculated surface temperature is positive, snow will melt and

the surface temperature is set to 0 °C (see more detailed description of snow dynamics in Section 2.5).

2.3. Vegetation

Vegetation influences energy and water exchanges between ground and the atmosphere, and influences soil moisture conditions as well. The plant canopy is modeled as a single layer whose energy balance (or energy conservation) includes the change of heat contained in the whole vegetation layer (Eq. 20). The heat capacity of the canopy is estimated based on plant biomass and its water content (Eq. 21).

The net solar radiation intercepted by the canopy is estimated based on vegetation area index (Eq. 22). Both the net long-wave radiation and sensible heat flux include exchanges with the HC upper surface and the above atmosphere (Eq. 23 and 24). The sensible heat flux between the canopy and the air above the canopy is more directly related with canopy surface temperature than canopy mean temperature. Measurements show that temperature in the upper part of the canopy is closer to the air temperature above the canopy [*Black et al., 1996*]. We estimate this canopy surface temperature as the average of canopy mean temperature and the air temperature above the canopy, which produces a factor of 0.5 in Eq. 24. Latent heat flux of canopy is estimated based on Penman-Monteith equation [*Monteith, 1965*] (Eq. 19) using canopy resistance instead of surface resistance. Canopy resistance is simulated based on the method from *Liu et al.* [*1999*], which includes the effects of radiation, air temperature, vapor pressure deficit, and leaf water potential on stomatal resistance. When there is intercepted water in the canopy, latent heat flux will consume this intercepted water, and canopy resistance is set to zero.

2.4. Soil water dynamics

Soil moisture influences soil thermal properties, and is also closely related to surface water and energy fluxes and snow processes. We simulate soil water dynamics considering water input, output and distribution among soil layers. Water input includes rainfall and snowmelt. We assume that precipitation is rainfall when air temperature is higher than 0 °C, otherwise the precipitation is snowfall [*Kongoli and Bland, 2000*]. Precipitation (rainfall or snowfall) is subject to canopy interception. The maximum canopy interception (Int_{max}) is estimated based on leaf area index (LAI) [*Verseghy et al., 1993*] Plant interception proceeds until Int_{max} is reached, after that, the excess

precipitation reaches the ground. Water infiltration is treated as a saturated flow from the upper soil layer downward. Water loss from soil includes soil evaporation (Eq. 19) and plant transpiration. Plant transpiration is the difference between plant evapotranspiration (canopy latent flux) and evaporation of canopy-intercepted water. Soil evaporation consumes water from the top layer first, proceeding through underlying layers until the requirement is satisfied. Transpiration consumes water in the layers of root zone according to the amount of water available for plant uptake in each layer (water content above wilting point).

Water transfer occurs only in mineral and organic soil layers. Water flux between layers is simulated based on water potential gradient (Eq. 25) [*Richards, 1931*]. Water vapor movement and liquid water movement in response to temperature gradients are ignored. Hydraulic conductivity and soil water suction are estimated based on soil moisture and soil texture (Eq. 26-29) [*Campbell, 1974; Clapp and Hornberger, 1978*]. The parameters (b, K_{WS} and ϕ_S) are estimated based on *Clapp and Hornberger* [*1978*] for mineral soils, and based on *Ogee and Brunet* [*2002*] and *Letts et al.* [*2000*] for forest floor and peat layers, respectively. When a soil layer is frozen, its hydraulic conductivity is set to zero [*William and Smith, 1989*]. More subtle processes, such as ice segregation and frost heaving are not considered in the model.

2.5. Snow dynamics

The snowpack is part of the profile for heat conduction. Both the thickness and the density of the snowpack are important for heat conduction, and the dynamics of snow are directly related with water dynamics and surface energy fluxes. We simulate the thickness of the snowpack based on the amount of snow on the ground (water equivalent) and snow density profile. The change of snow amount is the difference between snowfall and snowmelt. Snowfall is determined by precipitation and air temperature. The amount of snow intercepted by vegetation and loss by sublimation are estimated in the same way as for liquid water interception (Section 2.4). The amount of snowmelt is estimated based on the availability of energy [*Verseghy, 1991*]. If the solution of the surface energy balance equation results in a surface temperature (T_s) higher than 0 °C, energy is available for snowmelt on the surface. T_s is then reset to 0 °C and surface temperature related fluxes are recalculated, and the excess energy is used to estimate the amount of

snowmelt [*Verseghy, 1991*]. Snowmelt may also occur in the bottom of snowpack due to the heat conducted from the underlying ground. First we calculate the temperature (T'_l, is termed as apparent temperature) of the snow layers based on the heat conduction equation without considering the thawing/freezing effects. If T'_l >0 °C, the amount of energy available for snowmelt is estimated based on T'_l and the heat capacity of the layer, and the temperature of this layer is set to 0 °C. Melted water on the snow surface percolates to deeper layers after liquid water content is higher than its liquid water holding capacity [*Anderson, 1976*]. The liquid water holding capacity of a snow layer is estimated based on its density (Eq. 30) [*Kongoli and Bland, 2000*]. Water percolating to the bottom of the snowpack and snowmelt from the bottom of the snowpack supply water to the underlying soil. This water may infiltrate into soil or accumulate on the surface if the topsoil layer is frozen.

The density of fresh snow is estimated following *LaChapelle* [*1969*] (Eq. 31). The change of snow density for each layer is simulated considering compaction (Eq. 32) [*Mellor, 1964*] and destructive metamorphism (Eq. 33 and 34) [*Anderson, 1976; Kongoli and Bland, 2000*]. If melting is underway, Eq. 33 and 34 are multiplied by a parameter (C_{sp5}, with a value of 2) to account for the effects of liquid water [*Kongoli and Bland, 2000; Anderson, 1976*]. The model updates the thickness of the snowpack based the amount of snow (water equivalent) and its density profile every day, so that the upper boundary surface moves up and down according to snow dynamics.

2.6. Thawing and freezing

The internal heat source or sink term (or latent heat of fusion) in Eq. 1 is considered if thawing or freezing occurs. We assume thawing and freezing occur when temperature crosses 0 ºC. We simulated thawing and freezing of water in soil in a similar way as for snowmelt. First, we determine soil temperature of a layer without considering thawing and freezing processes (this temperature is called apparent temperature, T'_l); then, we consider the effects of thawing or freezing on the apparent temperature based on energy conservation: latent heat released or absorbed during freezing or thawing of a layer equals the amount of heat required or released for the apparent temperature change of the layer. For the thawing case (ice fraction f_{ice}>0 and T'_l >0 ºC), if the heat available ($C_l T'_l$) is less than thawing all the ice in this layer, soil temperature is set to 0 ºC and the fraction

of the ice reduced according to the energy available, otherwise all the ice will melt and the remain heat increases soil temperature. A similar procedure is conducted for the freezing process. The fractions of liquid water and ice in a layer are explicitly determined, and the heat capacity of the soil is updated in each time step (15-30 minutes) according to the fraction of liquid water and ice content. The depth of thawing or freezing is determined based on the fractions of liquid water and ice in soil layers (thawing and freezing front is within the layer where liquid water and ice coexist, and the thickness of freezing and thawing in a layer is interpolated based on the fractions of ice and liquid water in this layer).

2.7. Excess ground ice and ground subsidence

Excess ice often occurs in the upper layers of permafrost [*Williams and Smith, 1989*]. Deepening of ALT brings about ground ice melt and ground subsidence. Excess ice is defined as the volumetric ice content in soil over the moisture content at saturation [*Williams and Smith, 1989; Burn, 1998*], therefore, porosity of a layer is the sum of soil porosity defined by soil texture and the fraction of excess ice in this layer. In the model, the initial excess ice is an input parameter. The model calculates soil moisture (Section 2.4) and fractions of ice and liquid water in each layer (Section 2.6). When excess ice melts, water suction is set as 0 m, and hydraulic conductivity is set as the saturated hydraulic conductivity. We assume that ground subsidence occurs when the volume of moisture (liquid water and ice, given by Eq. 35) in a layer is less than the current porosity, and the current porosity is higher than the soil texture defined porosity (Eq. 36). After ground subsidence, the porosity of the layer is reduced accordingly. The model calculates ground subsidence on a daily basis, and the surface subsidence is the total subsidence of all the layers. Because ground subsidence is a slow process, we assume that the soil temperature profile simply shifts downward.

3. Model Validation

3.1. Approaches and data

We used three approaches to validate the model. First we tested the numerical scheme of the model under simplified conditions; then we selected four sites and compared the simulated results with the measurements, including the components of the energy

balance, snow depth, soil temperature and thaw depth; finally we tested the sensitivity of the model to the major input variables and parameters.

First, we tested the numerical scheme of the heat conduction without considering the surface energy processes and hydrological dynamics (except thawing and freezing processes). One case is from the Neumann solution for a step-increase in surface temperature, and another case is simulated by *Goodrich's* model [*1982*] under a sinusoidal change in surface temperature. The soil profile and the initial conditions were assumed uniform in distribution, and the heat flux from the lower boundary was set to zero. For the first case, the initial soil temperature and volumetric soil moisture were set as –5 ˚C and 0.4, respectively, and the surface temperature was 10 ˚C. For the second case, the initial soil temperature and volumetric soil moisture were set as –2 ˚C and 0.35, respectively, and the surface temperature followed a sinusoidal pattern with annual average of –2 ˚C and amplitude of 20 ˚C.

We then validated the model by comparing with the field measurements at four sites in Canada: two sites in Saskatchewan and two sites in Yukon Territory. The Saskatchewan sites were near the southern boundary of the permafrost region, about 50 km northwest of Prince Albert. One site (53.63 °N, 106.20 °W) was covered by deciduous forest of aspen (*Populus tremuloides*) with an understory of hazelnut (*Corylus cornuta Marsh*) (below referred as the OA site). LAI in summertime is 5.6 [*Black et al., 1996; Chen et al., 1999*]. The other site (53.92 °N, 104.69 °W) was a coniferous forest of jack pine (*Pinus Banksiana*) with LAI of 1.9 (winter) to 2.2 (summer) [*Baldocchi et al., 1997*] (below referred as the OJP site). We selected these two sites because detailed energy flux and temperature measurements were available. Detailed site conditions and measurements are described by *Black et al.* [*1996*], *Chen et al.* [*1999*], and *Baldocchi et al.* [1997]. Input climate data for NEST included air temperature, precipitation, vapor pressure (or relative humidity), wind speed, and solar radiation. Wind speed in the canopy was estimated as a function of wind speed above canopy and LAI, a relationship developed based on the measurements at the OA site. Table 2 shows the values of model parameters. Initial snowpack was determined based on the measurements on Jan. 20, 1994, when simulation began. Initial soil temperature was estimated using measurements on Jan. 20, 1994 for the upper layers (depth < 0.5 m). For deeper layers, the initial temperature was estimated

based on the general distribution patterns: From 0.5 to 10 m, initial soil temperature increased linearly to the annual mean at 10 m, where the inter-annual change of soil temperature was imperceptible [*Rieger, 1983*]; From 10 to 35 m, initial temperature increased with depth based on the geothermal gradient 0.015 °C·m^{-1} [*Jessop et al., 1984*]. Soil moisture was set to field capacity for the upper two-meters and saturated in deeper layers based on the general variation pattern of soil moisture [*Black et al., 1996*].

The Yukon sites (60.85 °N, 135.70 °W) were in Takhini River valley, about 50 km west of Whitehorse, and they were within the sporadic discontinuous permafrost zone. The valley was covered by forest before 1958. In July 1958, extensive forest fires burned most of the vegetation and the soil organic horizon, but about 1 km^2 of forest adjacent to a highway escaped burning. *Burn* [*1998*] measured soil temperature in this unburned area (below referred as the forested site) and at a nearby site in the burned area (below referred as the burned site). At the forested site, the ground was covered by 10 cm organic matter. The soil was composed of fine sands and fine-grained sediments (71% sand, 14% silt, and 15% clay). The excess ice content was about 20% below 150 cm at the forested site. The vegetation was medium to dense mature white spruce with few understories. At the burned site, the organic layer was burned during the fire, and there had been little regeneration of forest vegetation since the fire. Detailed site conditions are described by *Burn* [*1998*]. We simulated the soil temperature and thaw depth for the forested site and the burned site from 1955 to 1999 and compared with the measurements made by *Burn* [*1998*].

Climate data (from 1955 to 1999) were from the climate station at Whitehorse Airport, which was about 40 km from the measurement sites. Daily solar radiation was estimated based on extraterrestrial insolation and the transmission coefficient of solar radiation [*Spitters et al., 1986; Briston and Campbell, 1984*]. The diurnal variation of solar radiation was estimated from the daily solar radiation and a sine function [*Chung and Horton, 1987*]. The diurnal variation of temperature was derived from daily maximum and minimum temperatures [*William and Logan, 1981*]. Daily mean vapor pressure and wind speed were used without considering diurnal variations. For the forested site, the forest floor (10 cm depth) and vegetation conditions were constant for the simulation period from 1955 to 1999. LAI and plant biomass of the forest were estimated as 3.5 and

20 $kg \cdot m^{-2}$, respectively, based on typical mature forests around this area [*Chen J.M. et al., 2002*]. For the burned site, we changed the vegetation and forest floor conditions in 1958 considering the effects of fire (forested floor: 0 cm, summer LAI increased linearly from 0 to 1.0 during 1958 - 1999, biomass also increased linearly to 2 $kg \cdot m^{-2}$). The geothermal flux was 0.065 $W \cdot m^{-2}$ [*Jessop et al., 1984*]. Other parameters (root depth, plant water content, albedo and emissivity) were the same as for the Saskatchewan sites (Table 2). The initial daily climate data were derived by averaging the climate data for each day from 1955 to 1960 for temperature, vapor pressure and wind speed, and directly used the daily precipitation data in 1957, because the annual precipitation in this year is close to the long-term average at this site. The initial conditions were determined by iteratively running the model to equilibrium using the initial climate data.

Finally we tested the sensitivity of NEST to input climate drivers and other input parameters using the forested site in Yukon as the baseline. We ran the model to equilibrium (soil temperature and thaw depth are stable) after varying each climate driver and input parameter, and compared the output with the baseline results. The state variables selected for comparison included annual mean soil temperature at 50 cm depth (T_Y), monthly mean soil temperature in January (T_1) and in August (T_8) at 50 cm depth, and ALT.

3.2. Results and discussions

3.2.1. Comparing with the Neumann solution and the results from Goodrich's model

Figure 2A shows that the thaw depth simulated by NEST and the Neumann solution under a step-increase in surface temperature are very close to each other. We also simulate this case using Goodrich's model. The simulated thawing depth is very close to them as well, and the soil temperature profiles simulated by NEST and Goodrich's model agrees very well. For the case of the sinusoidal change in surface temperature, the simulated thawing depth by NEST is in good agreement with the results from Goodrich's model (Figure 2B). The soil temperature profiles simulated between these two models are also very close. Because Goodrich's model has been validated and compared with other numerical schemes [*Goodrich, 1982; Romanovsky et al., 1997*], these tests show that the numerical schemes of the NEST model for simulating heat conduction and thawing and freezing processes are valid.

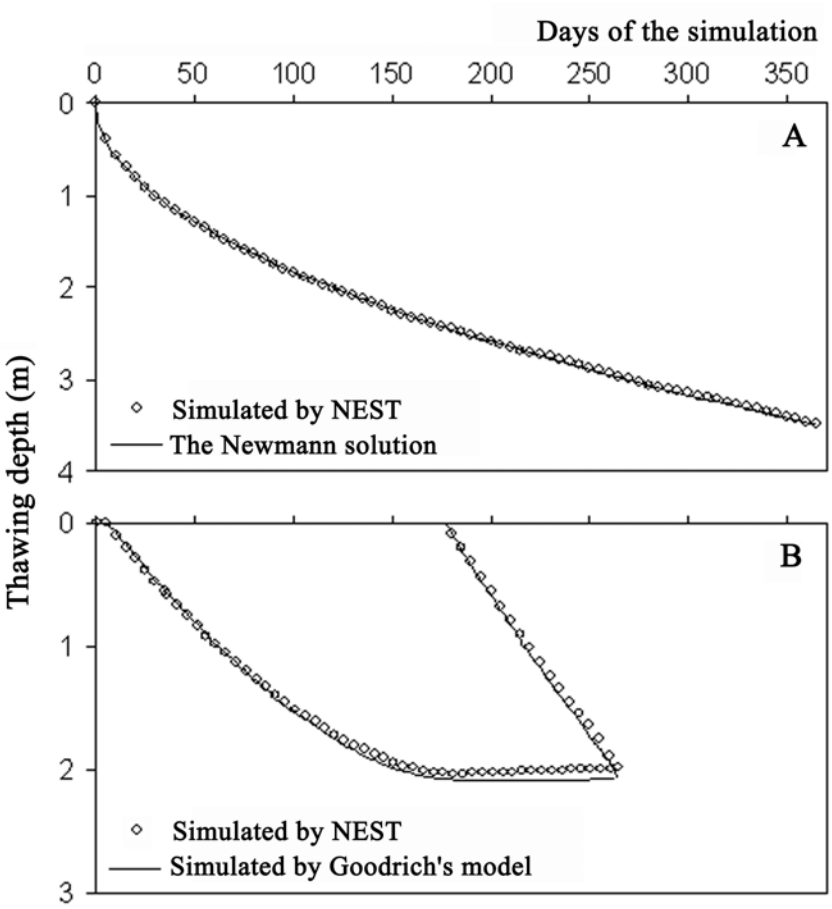

Figure 2. Comparisons between the simulated results by NEST with (A) the Neumann solution, and (B) the simulated results by Goodrich's model [*Goodrich, 1982*].

3.2.2. Comparing with field measurements

The Saskatchewan sites

Figure 3A shows a comparison between simulated and measured half-hourly canopy temperature at the OA site. We also include air temperature (input) for comparison. The simulated half-hourly canopy temperature is close to the measurements. Canopy temperature is higher than air temperature at mid-day, but lower during nighttime. The daily maximum air temperature lags about 1-2 hours compared to the daily maximum canopy temperature, but there is no significant timing difference between minimum air temperature and minimum canopy temperature. Figures 3B-D show comparisons between

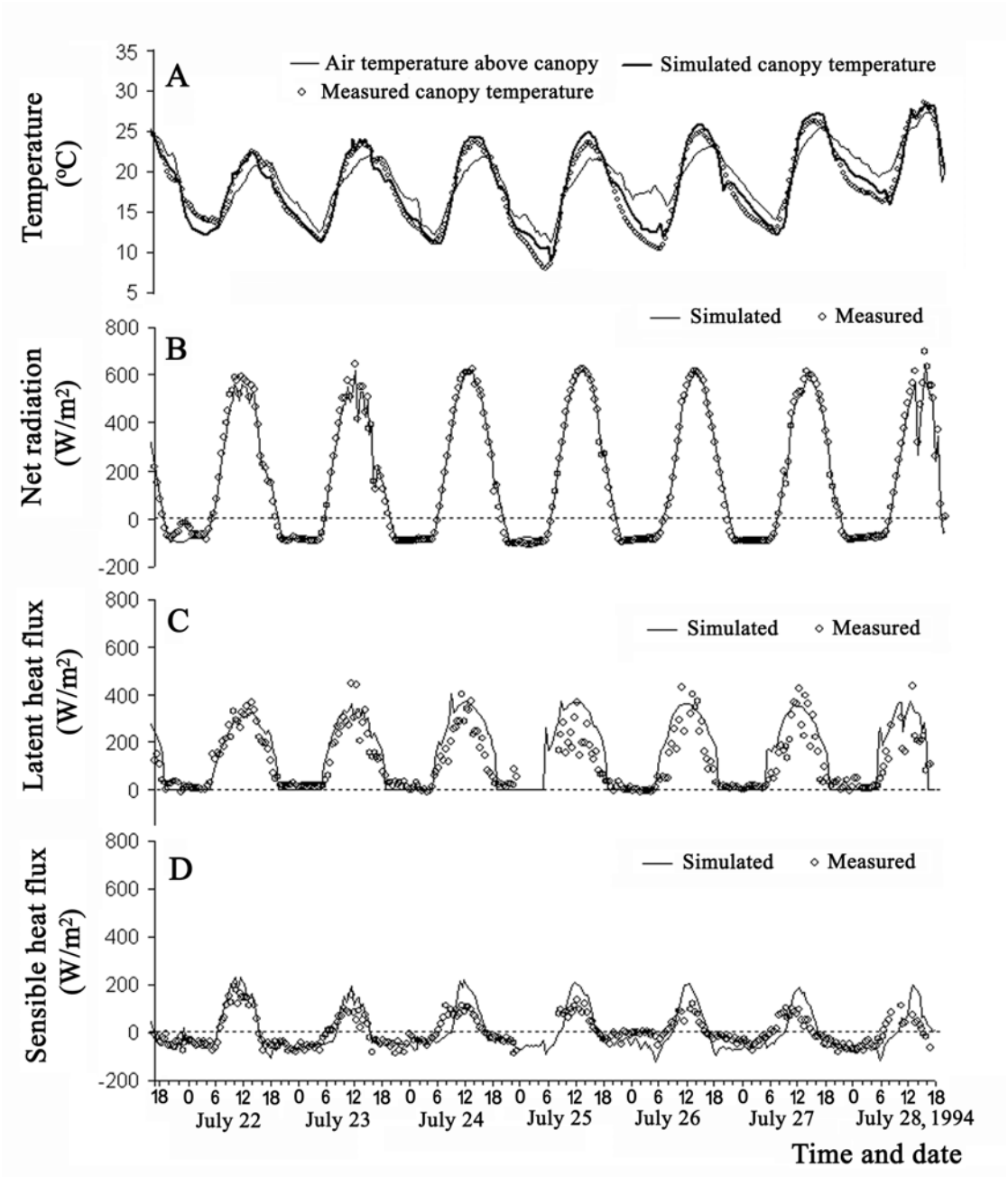

Figure 3. Comparisons between simulated and measured (A) canopy temperature, (B) net radiation, (C) latent heat flux above the canopy, and D) sensible heat flux above the canopy at the OA site in Saskatchewan.

simulated and measured net radiation, sensible and latent heat fluxes at the top of the canopy. The model captures the variation patterns of the energy fluxes. During daytime, about two-thirds of the net radiation is released as latent heat flux, and the remaining amount is released mainly as sensible heat. Figure 4 shows the variation patterns of the energy fluxes on the surface. The net radiation on the surface during daytime is only about 10% of that above the canopy, because of high leaf area index during this period. The closed canopy also limits sensible and latent heat fluxes between the surface and the canopy due to low wind speed and stable air stratification under the canopy. The simulated latent heat flux is lower than the measured values (measured at height of 0.45 m above the ground), perhaps because the measurements include some contributions from the understory below the observation level [*Blanken et al., 2001*]. These results show that the model captures the dynamics of energy fluxes above the canopy and between the surface and the canopy.

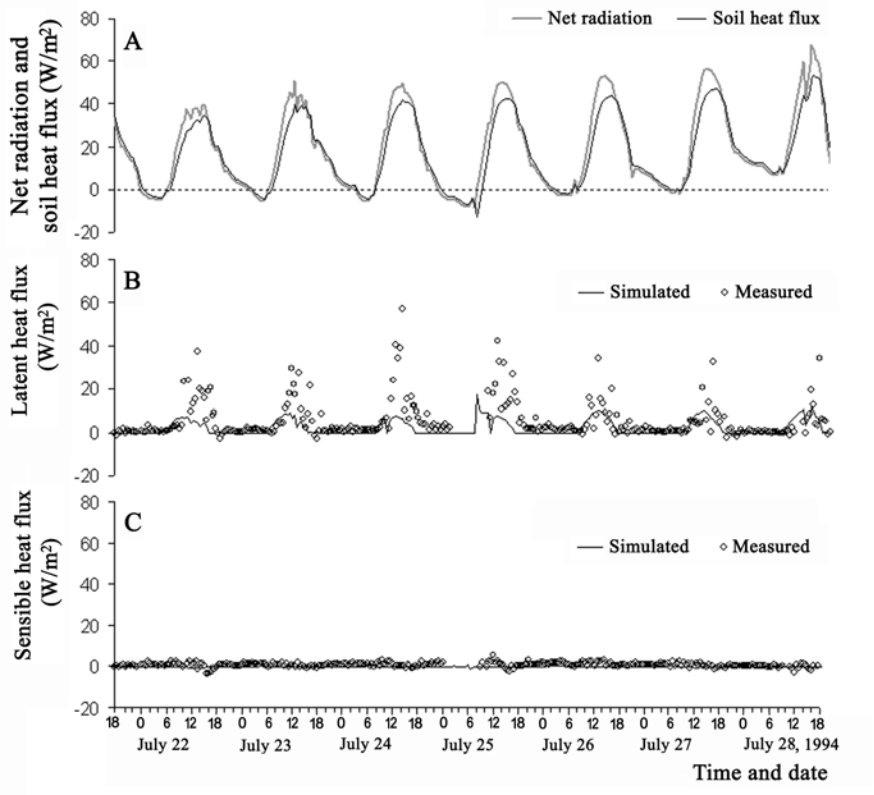

Figure 4. The energy fluxes on the soil surface at the OA site in Saskatchewan: (A) net radiation and soil heat flux (positive for downward), (B) latent heat flux, and (C) sensible heat flux. Latent and sensible heat fluxes were measured at 45 cm height above the ground. There were no measurements for net radiation and soil heat flux.

Figure 5 shows comparisons between simulated and measured daily snow depth and soil temperature at the OA site and the OJP site from Jan. 20, 1994 to Nov. 30, 1996. The simulated snow depth is in agreement with the measurements, and the model captures the difference between these two sites and the difference among these 3 years. The snow depth at the OJP site is slightly less than that at the OA site, largely due to the interception of snow by the canopy.

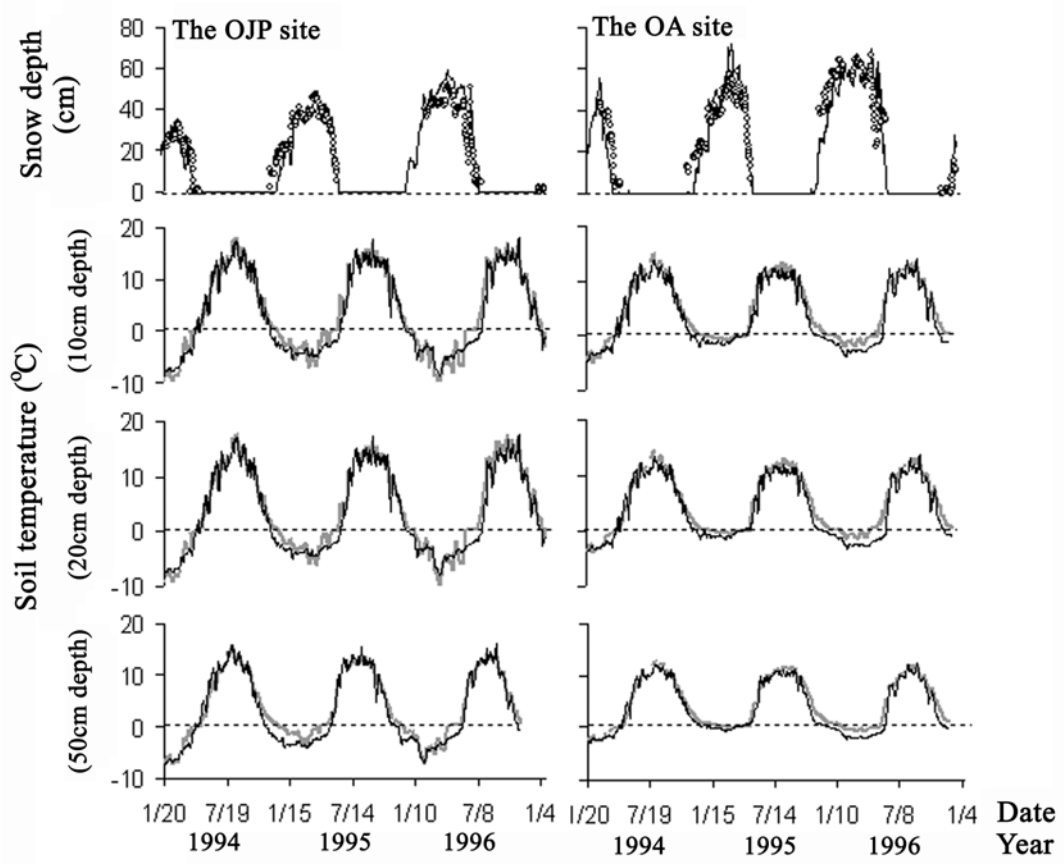

Figure 5. Comparisons between simulated and measured snow depth and soil temperature at 10 cm, 20 cm and 50 cm depths at the Saskatchewan sites. The thin black curves are simulated results, the circles are measured snow depth, and the thick gray curves are measured soil temperatures.

The simulated soil temperature is close to the measurements, and the model also captures the difference among these years and between these two sites. Although the snowpack is thicker and is present longer in 1995 than in the winter of 1994, soil temperature in the winter of 1995 is lower than in the winter of 1994, because the air

temperature in most of the winter in 1995 is about 10 °C lower than that in the winter of 1994. Soil temperature at the OJP site is lower than at the OA site in wintertime, but higher than at the OA site in summertime, mainly due to the combination effects of vegetation, forest floor, and snowpack: During summertime, the OA site has a denser canopy (LAI=6.5) than at the OJP site (LAI=2.4), so that less solar radiation reaches the ground at the OA site. In wintertime, more solar radiation reaches the surface at the OA site. The thicker forest floor at the OA site also lowers soil temperature in summertime, but increases soil temperature in wintertime. Simulated soil temperature is slightly lower than measured in winter of 1995 and spring of 1996, perhaps because the model underestimates snow accumulation in the early winter of 1995. The upper soil layers freeze and thaw annually, but there is no permafrost layer sustained at these two sites.

The Yukon sites

Figure 6 shows a comparison between simulated and measured daily snow depth from 1955 to 1999 at the burned site. The measurements are from the Whitehorse climate station. The model captures the general variation patterns (R^2=0.73, N=15551). The simulated snow depth at the forested site is similar to that of the burned site but slightly thinner mainly due to canopy interception of snowfall. Figure 7 shows a comparison between simulated and measured soil temperature at 1.5 m depth from 1991 to 1997 during which the measurements are available. The model captures the annual variation patterns and their difference between these two sites. Comparing to the burned site, the forested site has a lower soil temperature and smaller annual fluctuation, mainly due to vegetation and forest floor effects. Mean annual soil temperature at the burned site is about 0.8 °C higher than at the forested site at 1.5 m depth, and the increase of soil temperature at the burned site is more significant in the top layers. The soil temperature in upper layers responds quickly to forest fire (removal of vegetation and forest floor), but the response of ground temperature at 35 m depth takes several decades (Figure 8).

Figure 9 shows the simulated thaw depth from 1955 to 1999 for both the forested and the burned sites. *Burn* [*1998*] provided an annual change of thaw depth for 1993. Comparison of his measurements with the simulated results for this year (Figure 10) shows that the model captures the variation patterns of thaw depth at these two sites. The ALT at the burned site is about twice of the ALT at the forested site in 1993, although

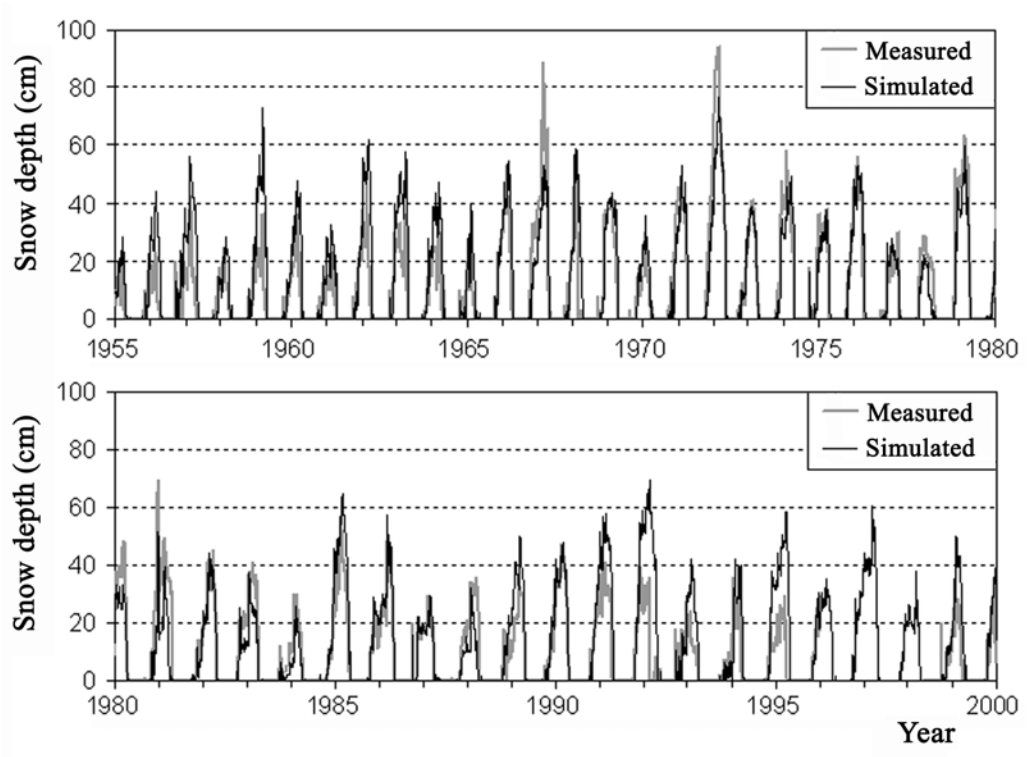

Figure 6. Comparisons between simulated and measured daily snow depth at the burned site in Yukon Territory. The measurements are from the Whitehorse airport climate station, Environment Canada.

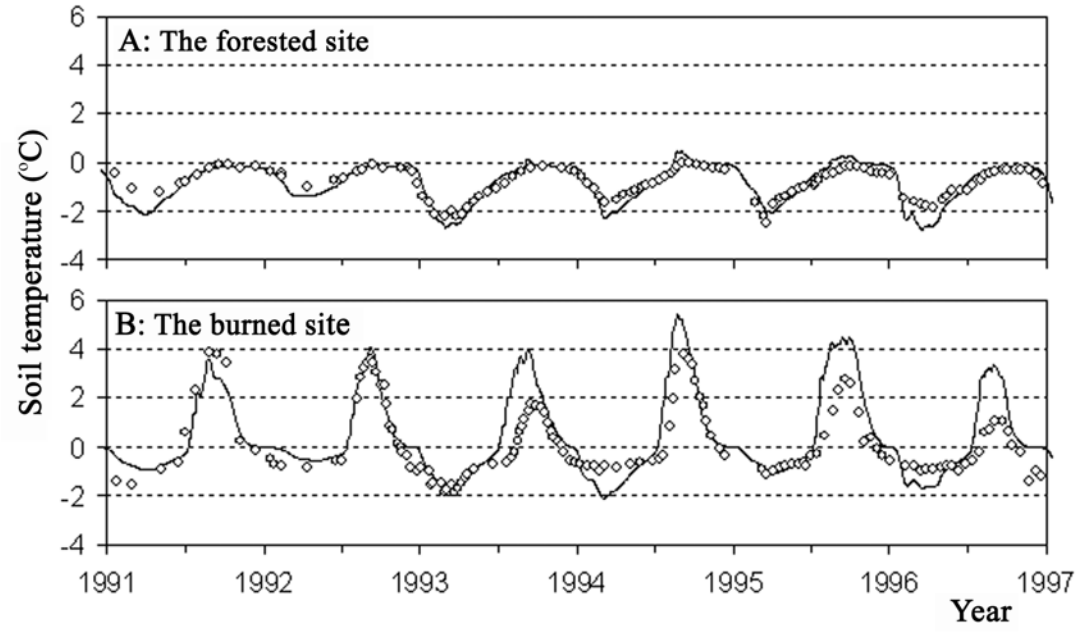

Figure 7. Comparisons between simulated (curves) and measured (circles) soil temperature at 1.5 m depth at the Yukon sites.

ALT changes with time and climate, especially at the burned site (Figure 9). At the forested site, ALT decreases about 30 cm from the 1950s to the 1970s, corresponding to air temperature decrease during this period (mean annual air temperature decreased about 3 °C). Thereafter ALT generally increases with some fluctuation from year to year (increased about 40 cm), corresponding to air temperature increase (annual mean air temperature increased by about 4 °C during this period). The overall variation of ALT is related to annual mean air temperature (R=0.42, n=45), especially with summertime (June to September) air temperature (R=0.63, N=45). At the burned site, ALT increases from 140 cm before forest fire to about 300 cm in the 1990s. This change includes the combination effects of climate and changes in vegetation and forest floor. Lacking the buffering of vegetation and forest floor at the burned site, ALT at this site is more sensitive to climate than at the forested site. The fluctuation of ALT from year to year at the burned site is 3 to 4 times larger than that at the forested site, and the increase in ALT after the mid 1970s is much more significant than at the forested site. Simulated ground subsidence at the forested site is small (about 1 cm), and only occurs in 1958 when summer temperature is the highest (which may have been a factor contributing to the forest fire in that year). Simulated accumulated ground subsidence at the burned site is about 33 cm, which is smaller than the thickness of ground ice in the increased active layer (40 cm for 200 cm increase in active-layer thickness and ground ice content of 20%). The water from the extra ground ice is still in the deep soil, so that ground subsidence will continue when this water is lost. This 45-year simulation exercise shows that the model can be used for long-term assessment for the effects of climatic change under different vegetation and ground conditions.

3.2.3. Sensitivity analysis

Table 3 shows the sensitivity of soil temperature and ALT to climate drivers and input parameters. Air temperature and solar radiation are the major climate variables influencing soil temperature and ALT. The effect of precipitation on wintertime temperature is more significant than on summertime temperature because of snow insulation. The model is not very sensitive to vapor pressure and wind speed. Forest floor depth, LAI, soil texture and light extinction coefficient are important local factors influencing soil temperature and ALT. Increasing forest floor depth increases soil

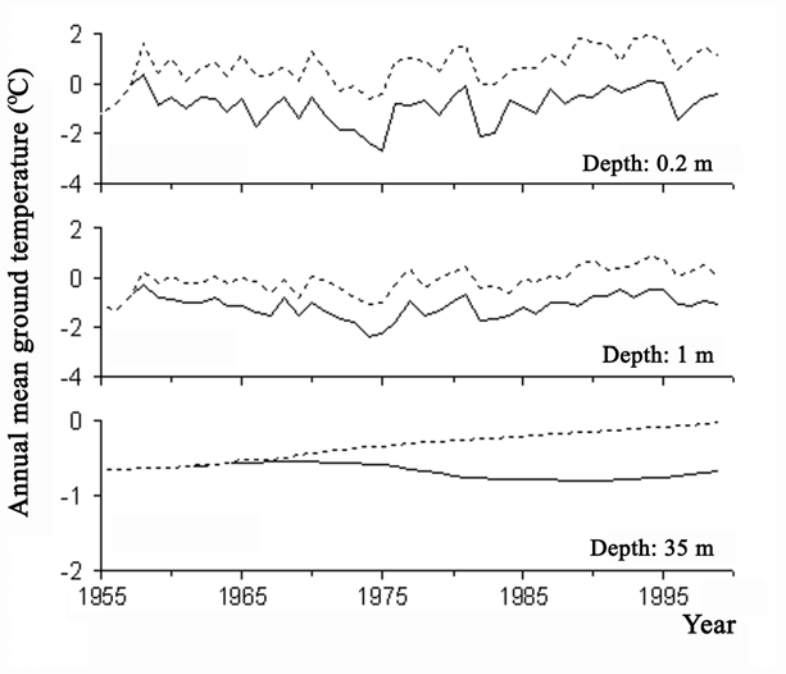

Figure 8. Comparison of annual mean soil temperature between the forested site (solid curves) and the burned site (dash curves) in Yukon Territory.

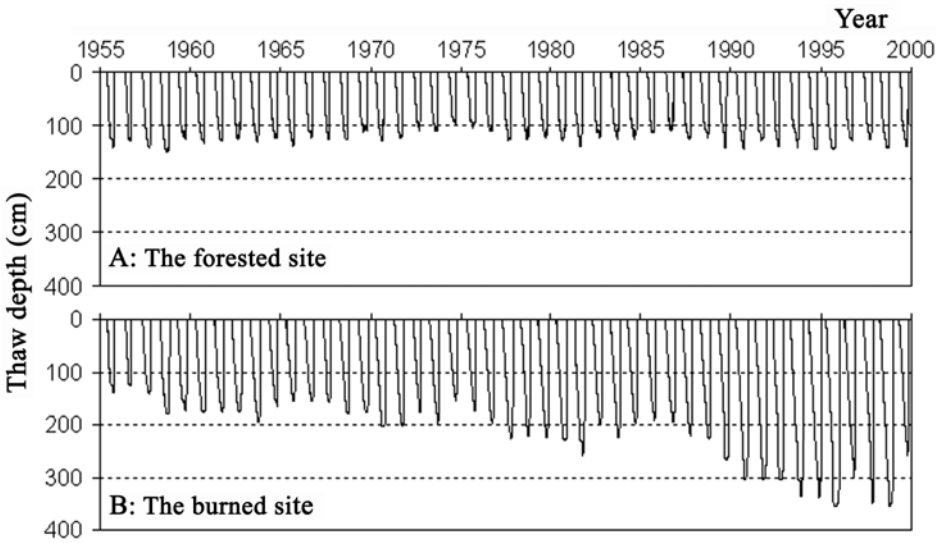

Figure 9. Simulated thawing depth for the Yukon sites. Forest fires occurred in July 1958 for the burned site.

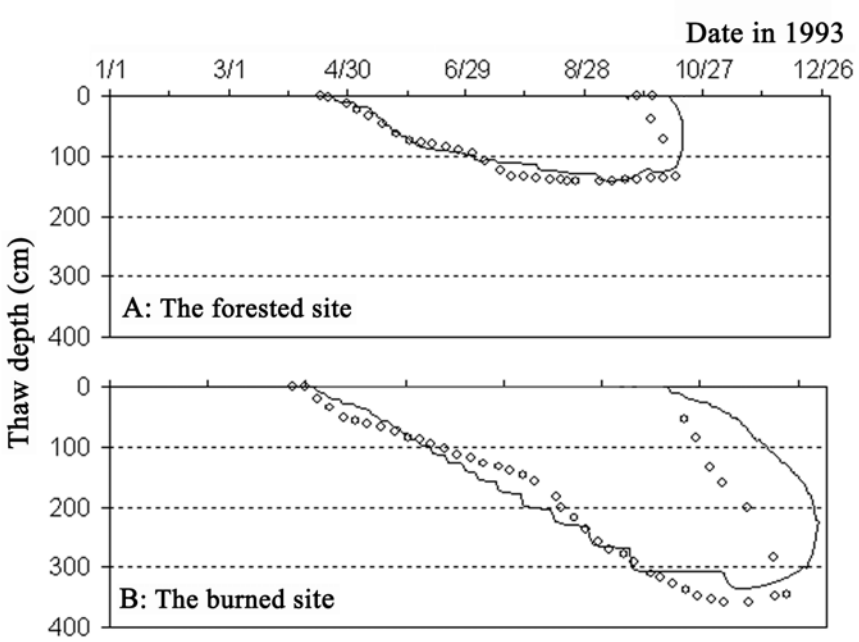

Figure 10. Comparisons between the simulated (curves) and measured (circles) thawing depth in 1993 for the Yukon sites.

temperature in wintertime due to its insulation effects, especially in this dry climatic condition (Annual mean precipitation is 260 mm from 1955-1999), but decreases soil temperature in summertime, therefore reducing ALT. Increasing LAI decreases soil temperature in both summertime and wintertime, mainly because of its shadowing effects on solar radiation. Changes in light extinction coefficient are equivalent to changes in LAI in their effects on radiation. Soil texture has a significant effect on ALT largely through its effects on hydrological dynamics. The simulated soil temperature (at 50 cm depth) and ALT are not very sensitive to the geothermal flux, lower boundary depth and soil depth at this site, but these factors, especially the geothermal flux, may affect the thickness of permafrost, and determine whether permafrost exists or not in southern margins of permafrost area. These results show that both climate and local conditions are important for soil temperature and ALT, and the responses of summertime and wintertime soil temperatures to input variables can be very different. Therefore, it is

essential to integrate climate and local conditions to predict the responses of soil temperature and ALT to climatic change.

4. Conclusions

A process-based model was developed to simulate soil temperature and thaw depth of northern ecosystems by combining the strength of existing permafrost models and land surface process models. Soil temperature and thawing depth were determined from solving the heat conduction equation, with the upper boundary conditions being determined using the surface energy balance and the lower boundary conditions being defined as the geothermal flux. This process-based approach allowed us to quantify and integrate the effects of climate, vegetation, ground features and hydrological conditions on ground thermal dynamics based on energy and water transfer in the soil-vegetation-atmosphere system. Testing against the measurements at four sites, we found good agreement between the simulated results and the measurements of energy fluxes, snow depth, soil temperature, and thaw depth. These results indicated that the model captured the physical processes of surface energy exchange, soil heat transfer, snow accumulation and melting, and soil thaw and freezing above permafrost or non-permafrost layers, as affected by climate, vegetation, and ground conditions. Therefore, this model can be used for investigating the impacts of transient climate change on soil thermal regimes and permafrost degradation, and their consequent effects on ecosystems and biogeochemical cycles under different vegetation and ground conditions.

Acknowledgement. The authors are very grateful to Sharon Smith and Daniel Riseborough for their suggestions about the model structure and their review and comments on the paper. Daniel Riseborough also provided Neumann solution and the simulation results from Goodrich's model for validation. The authors also thank Joost Van der Sanden for his critical internal review of this paper. The comments of three anonymous reviewers were very helpful in improving this manuscript. This project was supported by the Panel for Energy Research and Development (PERD), Canada's Climate Change Action Fund (CCAF), and the Long-Term Space Plan (LTSP).

Notation

b	an empirical parameter determined based on soil texture.
B_{Wood}	biomass of woody material of the canopy, $kg \cdot m^{-2}$.
C	soil heat capacity, $J \cdot m^{-3} \cdot °C^{-1}$.
C_c	heat capacity of canopy in a unit area, $J \cdot m^{-2} \cdot °C^{-1}$.
C_l,C_{l-1},C_{l+1}	soil heat capacity of layer l, $l-1$ and $l+1$, respectively, $J \cdot m^{-3} \cdot °C^{-1}$.
$C_{l,k}$	specific heat capacity of a constituent k in layer l, $J \cdot m^{-3} \cdot °C^{-1}$.
C_{pa}	specific heat capacity of air at constant pressure, $J \cdot kg^{-1} \cdot °C^{-1}$.
C_{sp1} to C_{sp5}	empirical parameters for snow dynamics, with the values of 0.01, 21, 0.0015, 0.04, and 2, respectively.
C_{water}	specific heat capacity of water, $J \cdot kg^{-1} \cdot °C^{-1}$.
C_{Wood}	specific heat capacity of dry wood, $J \cdot kg^{-1} \cdot °C^{-1}$.
D_l,D_{l-1},D_{l+1}	thickness of layer l, $l-1$ and $l+1$, respectively, m.
DS_{ice}	a ratio between the density of ice and water.
f_{Cloud}	fraction of cloud cover.
f_{Sky}	the sky view factor.
f_{ice}, f_w	fractions of ice and liquid water content in a soil layer, respectively.
f_{Water}	fraction of water content in plant.
F_W	water flux between soil layers, $m \cdot s^{-1}$.
g	the gravitational acceleration, 9.8 $m \cdot s^{-2}$.
$G_{l,l-1}$, $G_{l,l+1}$	the heat fluxes between layers l and $l-1$, and between layers l and $l+1$, respectively, $W \cdot m^{-2}$.
G_s	heat flux transmitted to the underlying layers from the surface, $W \cdot m^{-2}$.
GS_l	daily ground subsidence from layer l, m.
H_c	sensible heat lost from canopy, $W \cdot m^{-2}$.
H_s	sensible heat lost from the surface, $W \cdot m^{-2}$.
i	layer sequence number
Int_{max}	maximum canopy interception of precipitation, mm.
j	a number represents the soil constituents (1 to 5 for liquid water, ice, organic materials, minerals and air, respectively).
k	thermal conductivity, $W \cdot m^{-1} \cdot °C^{-1}$.
k_l, k_{l-1}, k_{l+1}	thermal conductivity of layers l, $l-1$ and $l+1$, respectively, $W \cdot m^{-1} \cdot °C^{-1}$.
$k_{l,,j}$	thermal conductivity of a constituent j in layer l, $W \cdot m^{-1} \cdot °C^{-1}$.
k_1	thermal conductivity of the top layer, $W \cdot m^{-1} \cdot °C^{-1}$.
k_v	von Karman's constant, 0.41.
K	extinction coefficient of solar radiation in canopy.
K_W	hydraulic conductivity, $m \cdot s^{-1}$.
K_{WS}	saturated hydraulic conductivity, $m \cdot s^{-1}$.
L_1	latent heat of ice fusion, 3.35×10^8 $J \cdot m^{-3}$ water.
L_c	latent heat lost from canopy, $W \cdot m^{-2}$.
L_s	latent heat flux of the surface, $W \cdot m^{-2}$.
m	a mid variable given by Eq. 28.
M	relative soil water content (relative to porosity).
M_i	relative water content at the infection point in soil moisture characteristic

Return to page 6
Go to Table 1

curve (0.92).

n	a mid variable given by Eq. 29.
LAI	leaf area index ($m^2 \cdot m^{-2}$).
P_{ol}	porosity of the soil layer l determined based on soil texture (volumetric fraction).
P_l	porosity of layer l (volumetric fraction).
r_{aa}	aerodynamic resistance between canopy and the air above the canopy, $s \cdot m^{-1}$.
r_{ac}	aerodynamic resistance between the HC surface and the canopy, $s \cdot m^{-1}$.
r_s	surface resistance for evaporation, $s \cdot m^{-1}$.
R_{lc}	net long-wave radiation of the canopy, $W \cdot m^{-2}$.
R_{sc}	solar radiation intercepted by canopy, $W \cdot m^{-2}$.
R_{ls}	net long-wave radiation on the HC surface, $W \cdot m^{-2}$.
R_{ns}	net radiation on the HC surface ($R_{ss} + R_{ls}$), $W \cdot m^{-2}$.
R_{s0}	incident solar radiation above the plant canopy, $W \cdot m^{-2}$.
R_{ss}	solar radiation accepted on the HC surface, $W \cdot m^{-2}$.
S	internal heat contribution due to freezing and thawing, $W \cdot m^{-3}$.
SLW	specific leaf weight, $kg \cdot m^{-2}$.
SW_l	volumetric fraction of soil moisture (including water and ice) in layer l without considering the volume changes during thawing and freezing.
t, t_h	time in units of seconds and in hours, respectively.
T	temperature, °C.
T_l, $T_{l,last}$	soil temperatures of the current and last time step, respectively, °C.
T_1	temperature of the top soil or snow layer (at mid point of the layer), °C.
T_a	air temperature above the canopy, °C.
T_c	canopy temperature, °C.
T_l,T_{l-1},T_{l+1}	temperatures of layers l, $l-1$, and $l+1$, respectively, °C.
T'_l	apparent temperature (calculated temperature without considering the effects of thawing and freezing) of layer l, °C.
T_s	surface temperature of the ground (no snow) or snowpack, °C.
T_{sp}	temperature of a snow layer, °C.
T_{spo},$T_{spc,}$	parameters for snow dynamics, with values of 0 °C for both of them.
u	wind speed above the canopy, $m \cdot s^{-1}$.
VAI	vegetation area index, $m^2 \cdot m^{-2}$.
VPD	vapor pressure deficit, mb.
V_{SWl}	volumetric fraction of moisture in soil layer l.
W_e	liquid water holding capacity of a snow layer, $g \cdot cm^{-3}$.
W_{em}, W_{eM}	parameters for the minimum and maximum water holding capacity of snow, 0.0 $g \cdot cm^{-3}$ and 0.1 $g \cdot cm^{-3}$, respectively.
W_{sp}	weight of the overlying snow above a layer in a unit area, $g \cdot cm^{-2}$.
Z	depth from the surface of ground or snowpack if snow is present, m.
z	a reference height above the canopy, m.
z_0	roughness height for the canopy, m.
z_d	zero plane displacement of the canopy, m.
α	albedo.

Return to page 6
Go to Table 1

δ	a mid variable given by Eq. 16.
ε	a mid variable given by Eq. 17.
ε_a, ε_c, ε_s	emissivity of air, vegetation and surface (soil or snow), respectively.
ε_{ad}	emissivity of the atmosphere in clear sky.
ρ_a	density of air, $kg \cdot m^{-3}$.
ρ_{ns}	density of fresh snow, $g \cdot cm^{-3}$.
ρ_{sp}, ρ_{spl}	density of a snow layer, $g \cdot cm^{-3}$.
ρ_{spd}	a threshold snow density used in Eq. 33 and 34, 0.15 $g \cdot cm^{-3}$.
ρ_{spe}	a threshold snow density used in Eq. 30, 0.2 $g \cdot cm^{-3}$.
$\theta_{l,j}$	volumetric fraction of a constituent *j* in layer *l*.
σ	Stefan-Boltzman constant, 5.7×10^{-8} $W \cdot m^{-2} \cdot K^{-4}$.
ϕ	soil water suction, m.
ϕ_i	soil water suction at the infection point in the soil moisture characteristic curve, m.
ϕ_S	soil water suction at saturation, m.
Δ	change rate of saturation vapor pressure with temperature, $mb \cdot K^{-1}$.
ΔT_l	temperature change of layer *l*, °C.
Δt	time step, s.
Υ	psychrometer constant, $J \cdot kg^{-1} \cdot K^{-1}$.

Return to page 6
Go to Table 1

References

Aber, J.D., P.B. Reich, and M.L. Goulden, Extrapolating leaf CO_2 exchange to the canopy: a generalized model of forest photosynthesis compared with measurements by eddy correlation, *Oecologia, 106,* 257-265, 1996.

Anderson, E.A., A point energy and mass balance model of snow cover, *NOAA technical report NWS 19,* 150 pp., US Department of Commerce, Silver Spring, MD, 1976.

Anisimov, O.A., Changing climate and permafrost distribution in the Soviet Arctic, *Physical Geography, 10,* 285-293, 1989.

Anisimov, O.A., N.I. Shiklomanov, and F.E. Nelson, Global warming and active-layer thickness: results from transient general circulation models, *Global and Planetary Change, 15,* 61-77, 1997.

Anisimov, O.A., and F.E. Nelson, Permafrost distribution in the Northern Hemisphere under scenarios of climatic change, *Global and Planetary Change, 14,* 59-72, 1996.

Anisimov, O., B. Fitzharris, J.O. Hagan, R. Jeffries, H. Marchant, F.E. Nelson, T. Prowse, and D.G. Vaughan, Polar regions (Arctic and Antarctic), in *Climate Change: Impacts, Adaptation, and Vulnerability, The Contribution of Working Group II of the Intergovernmental Panel on Climate Change*, Third Assessment Review, 801-841 pp., Cambridge, U.K., Cambridge University Press, 2001.

Baldocchi, D.D., C.A. Vogel, and B. Hall, Seasonal variation of energy and water vapor exchange rates above and below a boreal jack pine forest canopy, *J. Geophys. Res.,102,* 28939-28951, 1997.

Betts, A.K., and H.H. Ball, Albedo over boreal forest, *J. Geophys. Res., 102,* 28901-28909, 1997.

Black, T.A., G. den Hartog, H.H. Neumann, P.D. Blanken, P.C. Yang, C. Russel, Z. Nesic, X. Lee, S.G. Chen, R. Staebler, and M.D. Novak, Annual cycles of water vapor and carbon dioxide fluxes in and above a boreal aspen forest, *Global Change Biology, 2,* 219-229, 1996.

Blanken, P.D., T.A. Black, H.H. Neumann, G. den Hartog, P.C. Yang, Z. Nesic, and X. Lee, The seasonal water and energy exchange above and within a boreal aspen forest. *J. of Hydrology, 245,* 118-136, 2001.

Blanken, P.D., T.A. Black, H.H. Neumann, G. den Hartog, P.C. Yang, Z. Nesic, R. Staebler, W.J. Chen, and M.D. Novak, Turbulent flux measurements above and below the overstory of a boreal aspen forest, *Boundary-Layer Meteorol., 89,* 109-140, 1998.

Bonan, G.B., A computer model of the solar radiation, soil moisture, and soil thermal regimes in boreal forests, *Ecol. Model., 45,* 275-306, 1989.

Briston, K.L., and G.S. Campbell, On the relationship between incoming solar radiation and daily maximum and minimum temperature, *Agric. For. Meteorol., 31,* 159-166, 1984.

Brown, J., K.M. Hinkel, and F.E. Nelson, The circumpolar active layer monitoring (CALM) program: research designs and initial results, *Polar Geography, 24,* 166-252, 2000..

Brown, R.J.E., *Permafrost in Canada: Its Influence on Northern Development,* 234 pp., University of Toronto Press, Toronto, Canada, 1970.

Burgess, M.M., S.L. Smith, J. Brown, V. Romanovsky, and K. Hinkel, Global Terrestrial Network for Permafrost (GTNet-P): permafrost monitoring contributing to global climate observations, *Current Research 2000-E14,* 8 pp., Geological Survey of Canada, 2000.

Burn, C.R., The response (1958-1997) of permafrost and near-surface ground temperature to forest fire, Takhini River valley, southern Yukon Territory, *Can. J. Earth Sci., 35,* 184-199, 1998.

Burn, C.R., and M.W. Smith, Issues in Canadian permafrost research, *Progress in Physical Geography, 17,* 156-172, 1993.

Campbell, G.S., *An Introduction to Environmental Biophysics,* 150 pp., Springer-Verlag, New York, 1977.

Campbell, G.S., A simple method for determining unsaturated conductivity from moisture retention data, *Soil Sci., 117,* 311-314, 1974.

Chen, J.M., G. Pavolic, L. Brown, J. Cihlar, S.G. Leblanc, P.H. White, R.G. Hall, D. Peddle, D.J. King, J.A. Trofymow, E. Swift, J. van der Sanden, and P. Pellikka, Validation of Canada-wide leaf area index maps using ground measurements and high and moderate resolution satellite imagery, *Remote Sensing of Environment, 80,* 165-184, 2002.

Chen, W., Y. Zhang, J. Cihlar, S. L. Smith, and D.W. Riseborough, Changes in soil temperature and active-layer thickness during the 20th Century in a region in western Canada, *J. Geophys. Res.*, this issue.

Chen, W., T.A. Black, P.C. Yang, A.G. Barr, H.H. Neumann, Z. Nesic, P.D. Blanken, M.D. Novak, J. Eley, R.J. Ketler, and R. Cuenca, Effects of climatic variability on the annual carbon sequestration by a boreal aspen forest, *Global Change Biology, 5,* 41-53, 1999.

Chen, W., M.D. Novak, T.A. Black, and X. Lee, Coherent eddies and temperature structure functions for three contrasting surfaces. Part I: ramp model with finite microfront time, *Boundary-Layer Meteorology, 84,* 99-123, 1997a.

Chen, W., M.D. Novak, T.A. Black, and X.H. Lee, Coherent eddies and temperature structure functions for three contrasting surfaces. Part II: Renewal model for sensible heat flux, *Boundary-Layer Meteorol., 84,* 125-147, 1997b.

Choudhury, B.J., and J.L. Monteith, A four-layer model for heat budget of homogenous land surface, *Quarterly Journal of Royal Meteorological Society, 114,* 373-398, 1988.

Chung, S.O., and R. Horton, Soil heat and water flow with a partial surface mulch, *Water Resources Research, 23,* 2175-2186, 1987.

Clapp, R.B., and G.M. Hornberger, Empirical equations for some soil hydraulic properties, *Water Resources Research, 14,* 601-604, 1978.

Goodrich, L.E., The influence of snow cover on the ground thermal regime, *Can. Geotech. J., 19,* 421-432, 1982.

Goulden, M.L., S.C. Wofsy, J.W. Harden, S.E. Trumbore, P.M. Crill, S.T. Gower, T. Fries, B.C. Daube, S-M Fan, D.J. Sutton, A. Bazzaz, and J.W. Munger, Sensitivity of boreal forest carbon balance to soil thaw, *Science, 279,* 214-217, 1998.

Gower, S.T., J.G. Vogel, J.M. Norman, C.J. Kucharik, S.J. Steele, and T.K. Stow, Carbon distribution and aboveground net primary production in aspen, jack pine, and black spruce stands in Saskatchewan and Manitoba, Canada, *J. Geophys. Res., 102,* 29029-29041, 1997.

Houghton, J.T., L.G. Meira Filho, B.A. Callander, N. Harris, A. Kattenberg, and K. Maskell (Eds.), *Climate Change 1995: The Science of Climate Change, Contribution of Working Group I to the Second Assessment Report of the*

Intergovernmental Panel on Climate Change, 572 pp., Cambridge University Press, Cambridge, United Kingdom and New York, NY, USA, 1996.

Jessop, A.M., T.J. Lewis, A.S. Judge, A.E. Taylor, and M.J. Drury, Terrestrial heat flow in Canada, *Tectonophysics, 103,* 239-261, 1984.

Johansen, O., Thermal conductivity of soils, Ph.D. thesis, Trondheim, Norway, 1975.

Kane, D.L., L.D. Hinzman, and J.P. Zarling, Thermal response of the active layer to climatic warming in a permafrost environment, *Cold Regions Science and Technology, 19,* 111-122, 1991.

Kongoli, C.E., and W.L. Bland, Long-term snow depth simulation using a modified atmosphere-land model, *Agric. For. Meteorol., 104,* 273-287, 2000.

LaChapelle, E.R., Properties of snow, in *Hydrologic Systems,* 21 pp., College of Forest Resources, University of Washington, Seattle, 1969.

Letts, M.G., N.T. Roulet, N.T. Comer, M.R. Skarupa, and D.L. Verseghy, Parameterisation of peatland hydrological properties for the Canadian Land Surface Scheme, *Atmosphere-Ocean, 38,* 141-160, 2000.

Liu, J., J.M. Chen, J. Cihlar, and W. Chen, Net primary productivity distribution in the BOREAS study region from a process model driven by satellite and surface data, *J. of Geophys. Res., 104,* 27735-27754, 1999.

Malevsky-Malevich, S.P., E.K. Molkentin, E.D. Nadyozhina, and O.B. Shklyarevich, Numerical simulation of permafrost parameters distribution in Russia, *Cold Regions Science and Technology, 32,* 1-11, 2001.

Mellor, M., Engineering properties of snow, *J. of Glaciol., 19,* 15-66, 1977.

Monteith, J.L., Evaporation and environment, Symp. Soc. Exp. Biol. XIX, 205-234, 1965.

Nelson, F.E., (Un)frozen in time, *Science, 299,* 1673-1675, 2003.

Nelson, F.E., O.A. Anisimov, and N.I. Shiklomanov, Climate change and hazard zonation in the circum-arctic permafrost regions, *Natural Hazards, 26,* 203-225, 2002.

Nelson, F.E., O.A. Anisimov, and N.I. Shiklomanov, Subsidence risk from thawing permafrost, *Nature, 410,* 889-890, 2001.

Nelson, F.E., N.I. Shiklomanov, G.R. Mueller, K.M. Hinkel, D.A. Walker, and J.G. Bockheim, Estimating active-layer thickness over a large region: Kuparuk river basin, Alasa, U.S.A., *Arctic and Alpine Research, 29,* 367-378, 1997.

Nelson, F.E., Permafrost distribution in central Canada: Application of a climate-based predictive model, *Annals of the association of American Geographers, 76,* 550-569, 1986.

Oechel, W.C., S.J. Hastings, G. Vourlitis, M. Jenkins, G. Riechers, and N. Grulke, Recent change of Arctic tundra ecosystems from a net carbon dioxide sink to a source, *Nature, 361,* 520-523, 1993.

Ogee, J., and Y. Brunet, A forest floor model for heat and moisture including a litter layer, *J. of Hydrology, 255,* 212-233, 2002.

Oke, T.R., *Boundary Layer Climates,* 372 pp., Methuen, New York, 1978.

Patankar, S.V., *Numerical Heat Transfer and Fluid Flow,* 197 pp., McGraw-Hill, Toronto, 1980.

Richards, L.A., Capillary conduction of liquids in porous mediums, *Physics, 1,* 318-333, 1931.

Rieger, S., *The Genesis and Classification of Cold Soils,* 230 pp., Academic Press, Inc. New York, 1983.

Romanovsky, V.E., and T.E. Osterkamp, Thawing of the active layer on the coastal plain of Alaskan Arctic, *Permafrost and Periglacial processes, 18,* 1-22, 1997.

Romanovsky, V.E., T.E. Osterkamp, and N.S. Duxbury, An evaluation of three numerical models used in simulations of the active layer and permafrost temperature regimes, *Cold Regions Science and Technology, 26,* 195-203, 1997.

Sellers, P.J., R.D. Dickinson, D.A. Randall, A.K. Betts, F.G. Hall, J.A. Berry, G.J. Collata, A.S. Denning, H.A. Mooney, C.A. Nobre, N. Sato, C.B. Field, and A. Henderson-Sellers, Modeling the exchange of energy, water, and carbon between continentals and the atmosphere, *Science, 275,* 502-509, 1997.

Sellers, P.J., Y. Mintz, Y.C. Sud, and A. Dalcher, A simple bioshere model (SiB) for use within general circulation models, *J. of the Atmospheric Sciences, 43,* 505-531, 1986.

Serreze, M.C., J.E. Walsh, F.S. Chapin III, T. Osterkamp, M. Dyurgerov, V. Romanovsky, W.C. Oechel, J. Morison, T. Zhang, and R.C. Barry, Observational

evidence of recent change in the northern high-latitude environment, *Climatic Change, 46,* 159-207, 2000.

Smith, M.W., Microclimatic influences on ground temperatures and permafrost distribution, Mackenzie Delta, Northwest Territories, *Can. J. Earth Sci., 12,* 1421-1438, 1975.

Smith, S.L., and M.M. Burgess, Mapping the sensitivity of Canadian permafrost to climate warming, *Current research, 1998-E*, 163-191 pp., Geological Survey of Canada, 1998.

Smith, M.W., and D.W. Riseborough, Ground temperature monitoring and detection of climate change, *Permafrost and Periglacial Processes, 7,* 301-310, 1996.

Spitters, C.J.T., H.A.J.M. Toussaint, and J. Goudriaan, Separating the diffuse and direct component of global radiation and its implication for modelling canopy photosynthesis. Part I: components of incoming radiation, *Agric. For. Meteorol., 38,* 217-229, 1986.

Sun, S.F., Moisture and heat transport in a soil layer forced by atmospheric conditions, M.S. Thesis, University of Connecticut, 1982.

Trumbore, S.E., O.A. Chadwick, and R. Amundson, Rapid exchange between soil carbon and atmospheric carbon dioxide driven by temperature change, *Science, 272,* 393-395, 1996.

Unsworth, M.H., and J.L. Monteith, Geometry of long-wave radiation at the ground. I. Angular distribution of incoming radiation, *Quarterly Journal of Royal Meteorological Society, 101,* 13-24, 1975.

Verseghy, D.L., CLASS – a Canadian land surface scheme for GCMs. I. Soil model, *Intl. J. of Climatology, 11,* 111-133, 1991.

Verseghy, D.L., N.A. McFarlane, and M. Lazare, CLASS – a Canadian land surface scheme for GCMs. II. Vegetation model and coupled runs, *Intl. J. of Climatology, 13,* 347-370, 1993.

Waelbroeck, W., Climate-soil processes in the presence of permafrost: a systems modeling approach, *Ecol. Model., 69,* 185-225, 1993.

Wenger, K.F. (ed). *Forestry Handbook,* 2nd edition, 1135 pp., John Wiley & Sons, New York, 1984.

William, J.P., and J.A. Logan, A model for diurnal variation in soil and air temperature, *Agricultural Meteorology, 23,* 205-216, 1981.

Williams, P.J., and M.W. Smith, *The Frozen Earth: Fundamentals of Geocryology*, 306 pp., Cambridge University Press, New York, 1989.

Zhang, X., L.A. Vincent, W.D. Hogg, and A. Niitsoo, Temperature and precipitation trends in Canada during the 20th century, *Atmosphere-Ocean, 38,* 395-429, 2000.

Table 1. The equations of the model

Heat conduction in soil and snow profile

$$C\frac{\partial T}{\partial t}=\frac{\partial}{\partial Z}\left(k\frac{\partial T}{\partial Z}\right)+S \quad (1)$$

$$C_l\,\Delta T_l/\Delta t=\left(G_{l-1,l}-G_{l,l+1}\right)/D_l+S_l \quad (2)$$

$$G_{l-1,l}=\left(0.5k_l+0.5k_{l-1}\right)\left(T_{l-1}-T_l\right)/\left(0.5D_{l-1}+0.5D_l\right) \quad (3)$$

$$G_{l,l+1}=\left(0.5k_l+0.5k_{l+1}\right)\left(T_l-T_{l+1}\right)/\left(0.5D_{l+1}+0.5D_l\right) \quad (4)$$

$$C_l=\sum_{j=1}^{5}C_{l,j}\theta_{l,j} \quad (5)$$

$$k_l=\prod_{j=1}^{5}k_{l,j}^{\theta_{l,j}} \qquad \text{(Soil layers)} \quad (6)$$

$$k_l=0.074+2.576\rho_{spl}{}^2 \qquad \text{(Snow layers)} \quad (7)$$

The energy balance on the HC upper surface

$$R_{ls}+R_{ss}=H_s+L_s+G_s \quad (8)$$

$$R_{ss}=R_{s0}\left(1-\alpha\right)\exp\left(-K\cdot VAI\right) \quad (9)$$

$$R_{ls}=\sigma\varepsilon_s\left[\varepsilon_a\left(T_a+273\right)^4 f_{Sky}+\varepsilon_c\left(T_c+273\right)^4\left(1-f_{Sky}\right)-\left(T_s+273\right)^4\right] \quad (10)$$

$$\varepsilon_a=\left(1-0.84\,f_{Cloud}\right)\varepsilon_{ad}+0.84\,f_{Cloud} \quad (11)$$

$$\varepsilon_{ad}=0.72+0.005T_a \quad (12)$$

$$f_{Sky}=\exp\left(-K\cdot VAI\right) \quad (13)$$

$$H_s=\rho_a C_{pa}\left(T_s-T_a\right)/\left(r_{aa}+r_{ac}\right) \quad (14)$$

$$r_{aa}=\frac{\left[\ln\left(\left(z-z_d\right)/z_0\right)\right]^2}{k_v^2\,u}\left(1+\delta\right)^{\varepsilon} \quad (15)$$

$$\delta=\frac{5gz\left(T_c-T_a\right)}{\left(T_a+273.15\right)u^2} \quad (16)$$

$$\varepsilon=\begin{cases}-2 & \left(\delta\le 0\right)\\ -0.75 & \left(\delta>0\right)\end{cases} \quad (17)$$

$$G_s=k_1\left(T_s-T_1\right)/\left(0.5D_1\right) \quad (18)$$

$$L_s=\frac{\Delta\left(R_{ns}-G_s\right)+\rho_a C_{pa}VPD/r_{ac}}{\Delta+\gamma\left(1+r_s/r_{ac}\right)} \quad (19)$$

The energy balance of the canopy

$$R_{lc}+R_{sc}=H_c+L_c+C_c\cdot dT_c/dt \quad (20)$$

$$C_c=\left(C_{Wood}+f_{Water}C_{Water}\right)\left(B_{Wood}+LAI\cdot SLW\right) \quad (21)$$

$$R_{sc}=R_{s0}\left(1-\alpha\right)\left[1-\exp\left(-K\cdot VAI\right)\right] \quad (22)$$

$$R_{lc}=\sigma\left[\varepsilon_a\left(T_a+273\right)^4+\varepsilon_s\left(T_s+273\right)^4-2\left(T_c+273\right)^4\right]\left[\varepsilon_c\left(1-f_{Sky}\right)+\varepsilon_a f_{sky}\right] \quad (23)$$

$$H_c=0.5\rho_a C_{pa}\left(T_c-T_a\right)/r_{aa}-H_s \quad (24)$$

Soil water dynamics

$$F_W = K_W\left(\frac{d\phi}{dZ}+1\right) \tag{25}$$

$$K_W = K_{WS}M^{2b+3} \tag{26}$$

$$\phi = \begin{cases} \phi_s M^{-b} & (M < M_i) \\ -m(M-n)(M-1) & (M \geq M_i) \end{cases} \tag{27}$$

$$m = \frac{\phi_i}{(1-M_i)^2} - \frac{\phi_i b}{M_i(1-M_i)} \tag{28}$$

$$n = 2M_i - \frac{\phi_i b}{mM_i} - 1 \tag{29}$$

Snow dynamics

$$W_e = \begin{cases} W_{em} + (W_{eM} - W_{em})(\rho_{spe} - \rho_{sp})/\rho_{sp} & (\rho_{sp} \leq \rho_{spe}) \\ W_{em} & (\rho_{sp} > \rho_{spe}) \end{cases} \tag{30}$$

$$\rho_{ns} = \begin{cases} 0.05 + 0.017(T_a + 15)^{1.5} & (T_a > -15) \\ 0.05 & (T_a \leq -15) \end{cases} \tag{31}$$

$$\partial\rho_{sp}/\partial t_h = \rho_{sp} C_{sp1} \exp[-0.08(T_{sp0} - T_{sp})] W_{sp} \exp(-C_{sp2}\rho_{sp}) \tag{32}$$

$$\partial\rho_{sp}/\partial t_h = \rho_{sp} C_{sp3} \exp[-C_{sp4}(T_{spc} - T_{sp})] \quad (\rho_{sp} \leq \rho_{spd}) \tag{33}$$

$$\partial\rho_{sp}/\partial t_h = \rho_{sp} C_{sp3} \exp[-C_{sp4}(T_{spc} - T_{sp})] \exp[-46(\rho_{sp} - \rho_d)] \quad (\rho_{sp} > \rho_{spd}) \tag{34}$$

Ground subsidence

$$V_{SWl} = SW_l f_{wl} + SW_l(1 - f_{wl})/DS_{ice} \tag{35}$$

$$GS_l = \begin{cases} D_l(P_l - V_{SWl}) & (P_l > P_{0l}, P_l > V_{SWl}, \text{and } V_{SWl} \geq P_{0l}) \\ D_l(P_l - P_{0l}) & (P_l > P_{0l}, P_l > V_{SWl}, \text{and } V_{SWl} < P_{0l}) \\ 0 & (\text{other cases}) \end{cases} \tag{36}$$

Return to page 6
Go to notation page

Table 2. The model parameters for the Saskatchewan sites

Model parameters	The OA site	The OJP site
Latitude (°N)	53.63 [1]	53.92 [2]
Canopy height (m)	21.0 [1]	13.5 [2]
Woody biomass ($kg \cdot m^{-2}$)	18.5 [3]	6.7 [3]
Forest floor depth (cm)	9.0 [1]	5.7 [2]
Soil texture [4]	Silty clay [1]	Sandy [2]
Soil organic matter content (%)	3.8 [1]	1.5 [3]
Root zone depth (m)	0.6 [1]	0.6
Geothermal flux ($W \cdot m^{-2}$)	0.05 [5]	0.05 [5]
Albedo (no snowpack)	0.14 [6]	0.10 [6]
Albedo (with snowpack)	0.21 [6]	0.10 [6]
Water content in plant ($kg \cdot kg^{-1}$)	1.0 [7]	1.0 [7]
Specific leaf weight ($kg \cdot m^{-2}$)	0.1 [8]	0.28 [8]
Light extinction coefficient	0.58 [8]	0.50 [8]
The depth of soil (m)	5	5
Canopy emissivity	0.98 [9]	0.98 [9]
Soil emissivity	0.94 [9]	0.94 [9]
Snow emissivity	0.98 [9]	0.98 [9]

[1]*Black et al., 1996;* [2]*Baldocchi et al., 1997;* [3]*Gower et al., 1997;* [4]Soil moisture parameters *(b,* K_{WS} and ϕ_S) were determined based on soil texture according to *Clapp and Hornberger* [*1978*]; [5]*Jessop et al., 1984;* [6]*Betts and Ball, 1997;* [7]*Wenger, 1984;* [8]*Aber et al., 1996;* [9]*Oke, 1978.*

Return to page 12

Table 3. Sensitivity of soil temperature and ALT to input variables and parameters

Variables and parameters	Variation	ΔT_Y* (°C)	ΔT_1* (°C)	ΔT_8* (°C)	ΔALT* (cm)
Air temperature	+1°C	0.74	0.68	0.92	32.1
	-1°C	-0.89	-0.98	-0.79	-24.2
Precipitation	+20%	0.29	0.93	-0.01	4.1
	-20%	0.00	-0.23	0.16	2.4
Vapor pressure	+20%	0.04	0.08	0.02	0.5
	-20%	-0.04	-0.07	-0.03	-0.4
Wind speed	+20%	0.02	0.03	0.02	0.4
	-20%	-0.06	-0.09	-0.04	-0.9
Solar radiation	+20%	0.42	0.32	0.53	14.1
	-20%	-0.37	-0.27	-0.50	-14.1
Forest floor depth	+5cm	0.16	0.87	-0.40	-12.1
	-5cm	0.06	-0.36	0.51	11.8
LAI	+1 $m^2 \cdot m^{-2}$	-0.40	-0.51	-0.49	-14.7
	-1 $m^2 \cdot m^{-2}$	0.58	0.93	0.76	27.7
Soil texture	Sandy	-0.25	-1.01	0.35	33.2
	Clay	-0.17	-0.21	-0.19	-18.9
Light extinction coefficient	+20%	-0.28	-0.25	-0.41	-12.7
	-20%	0.34	0.22	0.47	12.7
Geothermal flux	0.01W$\cdot m^{-2}$	-0.08	-0.14	-0.07	-1.8
	0.15W$\cdot m^{-2}$	0.13	0.23	0.16	4.7
Lower boundary depth	55 m	0.03	0.06	0.03	0.8
	75 m	0.07	0.12	0.07	1.9
Soil depth	2.5 m	-0.00	0.00	-0.01	-0.3
	10 m	0.25	0.44	0.07	2.5

* ΔT_1, ΔT_8, ΔT_Y, and ΔALT are changes of soil temperature at 50cm depth for January, August and the whole year, and the changes of ALT, respectively, comparing to the baseline conditions.

Return to page 21